Strain Influence on the Oxygen Electrocatalysis of the (100)-Oriented Epitaxial La2NiO4+δ Thin Films at Elevated Temperatures

ARTICLE *in* THE JOURNAL OF PHYSICAL CHEMISTRY C · SEPTEMBER 2013

Impact Factor: 4.77 · DOI: 10.1021/jp404121p

10 AUTHORS, INCLUDING:

Dongkyu Lee
Massachusetts Institute of Technology
21 PUBLICATIONS **84** CITATIONS
SEE PROFILE

Alexis Grimaud
Collège de France
26 PUBLICATIONS **373** CITATIONS
SEE PROFILE

Habib
King Fahd University of Petroleum and Minerals
165 PUBLICATIONS **1,486** CITATIONS
SEE PROFILE

Michael D. Biegalski
Oak Ridge National Laboratory
129 PUBLICATIONS **2,507** CITATIONS
SEE PROFILE

THE JOURNAL OF PHYSICAL CHEMISTRY C

Feature Article

pubs.acs.org/JPCC

Strain Influence on the Oxygen Electrocatalysis of the (100)-Oriented Epitaxial $La_2NiO_{4+\delta}$ Thin Films at Elevated Temperatures

Dongkyu Lee,[†] Alexis Grimaud,[†] Ethan J. Crumlin,[†] Khaled Mezghani,[‡] Mohamed A. Habib,[‡] Zhenxing Feng,[†] Wesley T. Hong,[†] Michael D. Biegalski,[§] Hans M. Christen,[§] and Yang Shao-Horn*,[†]

[†]Electrochemical Energy Laboratory, Massachusetts Institute of Technology, 77 Massachusetts Avenue, Cambridge, Massachusetts 02139, United States

[‡]Mechanical Engineering Department, King Fahd University of Petroleum and Minerals, P.O. Box 279, Dhahran 31261, Saudi Arabia

[§]Center for Nanophase Materials Sciences, Oak Ridge National Laboratory, Oak Ridge, Tennessee 37831, United States

Supporting Information

ABSTRACT: Ruddlesden–Popper materials such as $La_2NiO_{4+\delta}$ (LNO) have high activities for surface oxygen exchange kinetics promising for solid oxide fuel cells and oxygen permeation membranes. Here we report the synthesis of the $(100)_{tetragonal}$-oriented epitaxial LNO thin films prepared by pulsed laser deposition. The surface oxygen exchange kinetics determined from electrochemical impedance spectroscopy (EIS) were found to increase with decreasing film thickness from 390 to 14 nm. No significant change of the surface chemistry with different film thicknesses was observed using ex situ auger electron spectroscopy (AES). Increasing volumetric strains in the LNO films at elevated temperatures determined from in situ high-resolution X-ray diffraction (HRXRD) were correlated with increasing surface exchange kinetics and decreasing film thickness. Volumetric strains may alter the formation energy of interstitial oxygen and influence on the surface oxygen exchange kinetics of the LNO films.

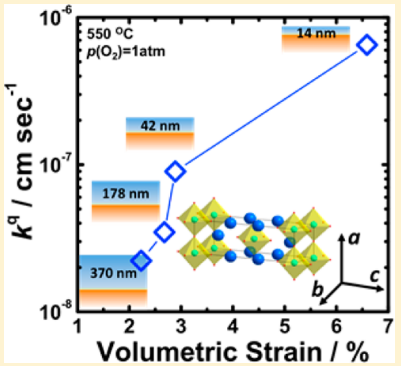

INTRODUCTION

Transition metal oxides such as $La_{1-x}Sr_xMnO_{3-\delta}$ (LSM)[1−5] are commonly used to promote oxygen electrocatalysis for solid oxide fuel cells[6−12] and oxygen permeation membrane applications[13] at high temperatures such as 1000 °C. Reducing the operating temperature is of vital importance to reduce the degradation and improve the lifetime of these solid-state devices. Mixed ionic and electronic conductors (MIECs) such as $La_{1-x}Sr_xCoO_{3-\delta}$ (LSC)[14−20] have been studied intensively to promote oxygen electrocatalysis at intermediate temperatures such as 600 °C. These MIECs have high surface oxygen exchange kinetics, which can allow oxygen electrocatalysis to take place on the entire oxide surface not just at the electrode/electrolyte interface. Ruddlesden–Popper (RP) oxides such as $La_2NiO_{4+\delta}$ (LNO) with high surface oxygen exchange kinetics and oxygen transport properties[21−30] are interesting alternative materials to LSC for intermediate temperature operation.[14−20] The RP structure can be described as an intergrowth of alternative NiO_2 and La_2O_2 rock salt layers or layers of LNO separated by LaO layers along the c axis, where oxygen transport kinetics by interstitial oxygen are considerably higher in the $a-b$ plane, up to 2 orders of magnitude, than along the c-axis.[21,23]

Although surface oxygen exchange kinetics of bulk RP oxides are well studied,[21,22,28,30] few studies have examined the anisotropic nature of the oxygen exchange kinetics in these oxides, which requires the use of single-crystalline samples.[15−17,31,32] Bassat et al.[21] have shown that the surface exchange kinetics in the $a-b$ plane is ∼5 times greater than that along the c-axis using LNO single crystals. Employing $(001)_{tetragonal}$-oriented epitaxial LNO thin films grown on the $(001)_{cubic}$-$SrTiO_3$ (STO) and $(110)_{cubic}$-$NbGaO_3$ (NGO) substrates, Burriel et al.[23] have shown that the surface oxygen kinetics in the $a-b$ plane is 2 orders of magnitude greater than that along the c-axis from secondary ion mass spectroscopy (SIMS) measurements. It is not clear if such a large anisotropy in the surface oxygen exchange kinetics found in these LNO films is intrinsic to LNO as the surface oxygen kinetics along the c-axis in these thin films are much lower than single crystals, while the values in the $a-b$ planes of LNO films are comparable. It is interesting to note that decreasing the compressive strains in the thin films on the NGO substrate with increasing film thickness increases oxygen transport kinetics but has no apparent influence on the surface exchange kinetics. This is in contrast to recent studies[15,17,33] revealing that strains in the epitaxial thin films and different film stoichiometry can greatly influence surface exchange kinetics. For example, Yamada et al.[33] have shown that compression in the c-axis of the $(110)_{tetragonal}$-oriented epitaxial $Nd_2NiO_{4+\delta}$ (NNO) film on

Received: April 26, 2013
Revised: August 16, 2013
Published: August 20, 2013

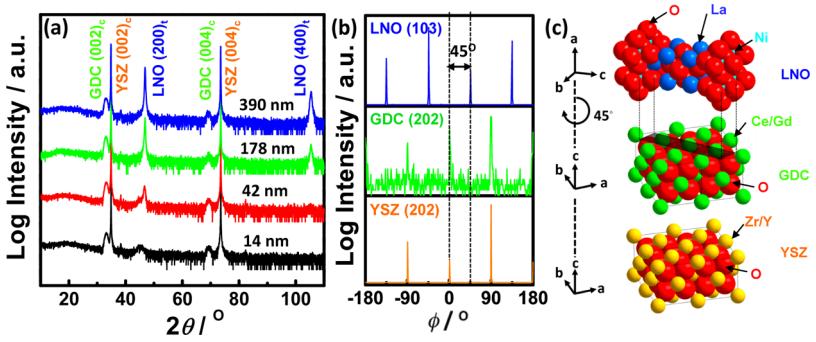

Figure 1. High-resolution X-ray diffraction (Cu K_α) analysis. (a) Normal XRD of the $(100)_{tetragonal}$-oriented epitaxial LNO thin films (~14, ~42, ~178, and ~390 nm), (b) off-normal XRD of the $(100)_{tetragonal}$-oriented epitaxial LNO thin films (~14 nm), GDC and YSZ, and (c) schematic of the crystallographic rotational relationships among the LNO $(200)_{tetragonal}$, GDC $(002)_{cubic}$, and YSZ $(002)_{cubic}$.

the $(100)_{cubic}$-Y_2O_3-stabilized ZrO_2 (YSZ) substrate reduces the surface exchange kinetics.

In this study, we report strong film thickness dependence on the surface oxygen exchange rates (k^q) of the $(100)_{tetragonal}$-oriented epitaxial growth of LNO thin films grown on YSZ in contrast to $(001)_{tetragonal}$-oriented epitaxial growth of LNO films.[23] Using in situ high-resolution X-ray diffraction (HRXRD), we show that the unit cell volume of the films increases as a function of increasing film thickness at elevated temperatures. As ex situ auger electron spectroscopy (AES) reveals no apparent difference in the surface chemistry of the LNO thin films upon heating, the thickness-dependent surface oxygen exchange rates of the LNO thin films can be attributed to different stains in these films.

EXPERIMENTAL METHODS

Pulsed laser deposition (PLD) was utilized to deposit the $(100)_{tetragonal}$-oriented epitaxial LNO thin films (~14, ~42, ~178, ~390 nm) on YSZ with gadolinium-doped ceria (GDC, 20 mol % Gd) as the buffer layer with thickness ~5 nm. Single-crystal 9.5 mol % Y_2O_3-stabilized ZrO_2 (YSZ) wafers with (001) orientation and dimensions of 10 × 5 × 0.5 mm (MTI corporation, USA) were used as substrate. Prior to LNO and GDC deposition, platinum ink (Pt) (#6082, BASF, USA) counter electrodes were painted on one side of the YSZ and dried at 900 °C in air for 1 h. The YSZ wafer was affixed to the PLD substrate holder using a small amount of silver paint (Leitsilber 200, Ted Pella, USA) for thermal contact. PLD was performed using a KrF excimer laser at λ = 248 nm, 10 Hz pulse rate, and 45 mJ pulse energy under $p(O_2)$ of 6.6×10^{-5} atm (50 mTorr) with 500 pulses of GDC (~5 nm) at 550 °C, followed by 1000 pulses, 5000 pulses, 15 000 pulses, and 35 000 pulses of LNO (~14, ~42, ~178, and ~390 nm, respectively) at 650 °C. The film thicknesses were determined by atomic force microscopy (AFM). The utilization of reflection high-energy electron diffraction (RHEED) enabled diagnostic in situ monitoring of the LNO film growth. After completing the LNO deposition, the sample was cooled to room temperature in the PLD chamber for ~1 h under an oxygen partial pressure of 6.6×10^{-5} atm (50 mTorr). The synthesis details of LNO and GDC PLD targets can be found in the Supporting Information (SI). Oxide phase purity and orientation of the thin-film systems were investigated via high-resolution X-ray diffraction (HRXRD) using a four-circle diffractometer (Panalytical, USA and Bruker D8, Germany). Measurements were performed in normal and off-normal configurations. LNO in the Ruddlesden–Popper structure is known to be orthorhombic with space group *Fmmm* at room temperature for an oxygen overstoichiometry (δ) ~ 0.18 as reported by Jorgensen et al.[34] As the Ruddlesden–Popper structure can be influenced greatly by the oxygen stoichiometry, fully oxidized $La_2NiO_{4.25}$ exhibits a monoclinic symmetry with space group *C*2 at room temperature,[35] while fully stoichiometric La_2NiO_4 is orthorhombic with space group *Bmab*.[36] In this study, large experimental uncertainty exists in the inferred oxygen non-stoichiometry of LNO thin films from the literature[37] using the lattice parameters determined from HRXRD (for details see the Supporting Information), and the XRD data of single-crystalline thin films do not allow a precise refinement of the symmetry of the LNO structure. Therefore, we chose the tetragonal symmetry with space group *I*4/*mmm*, which differs from the orthorhombic by the loss of the octahedral tilting (≤1°) in this study. The LNO in-plane lattice parameter (*b* and *c* lattice parameter) was determined from the off-normal $(114)_{tetragonal}$ and $(103)_{tetragonal}$ peak position, respectively, and the *a* lattice parameter of LNO normal to the film surface was determined from the $(200)_{tetragonal}$ peak positions. Surface morphology was examined by optical microscopy (Carl Zeiss, Germany) and atomic force microscopy (AFM) (Veeco, USA). AFM images of LNO films are shown in Figure S4 (SI).

In situ electrochemical impedance spectroscopy (EIS) measurements of microelectrodes ~200 μm in diameter were performed using a microprobe station (Karl Süss, Germany) connected to a frequency response analyzer (Solartron 1260, USA) and dielectric interface (Solartron 1296, USA). Temperature was controlled at 550 °C with heating stage (Linkam TS1500, UK), and data were collected between 1 MHz and 1 mHz using a voltage amplitude of 10 mV. EIS testing temperature was calibrated with a thermocouple contacting the thin-film surface, and deviation of ±5 °C was observed. EIS experiments were completed between $p(O_2)$ of 10^{-3} atm and 1 atm. EIS data were analyzed using an equivalent circuit (Figure S6(b), SI), from which the ORR resistance (R_{ORR}) and surface oxygen exchange rate were obtained. EIS data of all samples used in this study were found to be very similar in shape, and the detailed Nyquist plot of the $(100)_{tetragonal}$-oriented epitaxial LNO thin films with ~14 nm at 550 °C is shown in Figure S6(c) (SI).

In situ HRXRD was performed on a four-circle diffractometer (Panalytical) in an oxygen partial pressure of 1 atm and a controlled temperature stage (DHS 900, Anton Paar). Silver paste was used to adhere the thin-film sample to the heating plate. The heating rate was ~10 °C min^{-1}, and the temperature was held for 20 min at each temperature (25, 150, 250, 350,

dx.doi.org/10.1021/jp404121p | J. Phys. Chem. C 2013, 117, 18789–18795

450, and 550 °C) before XRD data were collected. Sample realignment was conducted at each temperature to maximize the XRD intensities. A full range θ–2θ normal scan was collected, and then high-resolution θ–2θ normal scans of LNO $(200)_{tetragonal}$ and YSZ $(002)_{cubic}$ were collected. Finally, high-resolution off-normal scans of LNO $(103)_{tetragonal}$, LNO $(114)_{tetragonal}$, and YSZ $(202)_{cubic}$ peaks were obtained. As the thermocouple for this experiment was placed inside the heating stage, a small difference between set and actual temperatures on the sample surface cannot be ruled out.

Ex situ auger electron spectroscopy (AES) was conducted with the Physical Electronics 700 Scanning Auger Nanoprobe (PHI, USA) operating at an accelerating voltage of 10 kV to analyze the surface chemistry change of the LNO films after heat treatment. The films were annealed at 550 °C for 6 h in an oxygen partial pressure of 1 atm before AES data were collected. The AES data were collected from three different locations (10 μm × 10 μm) selected on a sample in an ultra high vacuum chamber. Details about AES measurements can be found in the SI.

RESULTS AND DISCUSSION

Normal X-ray diffraction (XRD) data (Figure 1(a)) of LNO films collected at room temperature clearly show the presence

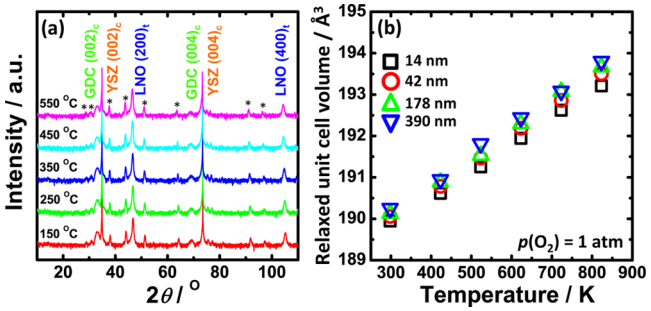

Figure 2. Structural stability and unit cell volume of the $(100)_{tetragonal}$-oriented epitaxial LNO thin films. (a) In situ HRXRD data (Cu K_α) of a normal scan in the θ–2θ Bragg–Brentano geometry as a function of temperature with ∼178 nm LNO film, showing no phase change upon heating at a $p(O_2)$ of 1 atm. The starred (*) peaks originated from the heater, and the peaks of the LNO film, GDC buffer layer, and YSZ substrate are indexed to the tetragonal, cubic, and cubic structure, respectively. (b) In situ HRXRD data of the unit cell volume of the $(100)_{tetragonal}$-oriented epitaxial LNO thin films with ∼14, ∼ 42, ∼178, and ∼390 nm as a function of temperature in a $p(O_2)$ of 1 atm.

of the $(l00)_{tetragonal}$ (l is even) peaks of LNO and $(00l)_{cubic}$ (l is even) peaks of GDC and YSZ, which indicates the synthesis of $(200)_{tetragonal}$-oriented LNO films having $(200)_{tetragonal}$LNO//$(002)_{cubic}$GDC//$(002)_{cubic}$YSZ. Off-normal phi-scan analysis (Figure 1(b)) allowed us to identify the in-plane crystallographic relationships between LNO, GDC and YSZ, and LNO and GDC, as shown in Figure 1(c). The data showed that $\langle 200\rangle_{tetragonal}$LNO was rotated by 45° with respect to the $\langle 002\rangle_{cubic}$GDC, which is expected due to lattice matching: $c(\text{LNO}) \approx 3\sqrt{2}/2a$ (GDC). The measured lattice parameters a and b of the LNO films were found to be nearly identical (a = 3.939 Å and b = 3.932 Å for 390 nm at RT, details about all measured lattice parameters in Figure S1, Supporting Information), which is in reasonably good agreement with literature data (a = 3.864 Å and b = 3.867 Å for the $(001)_{tetragonal}$-oriented epitaxial LNO thin film with ∼330

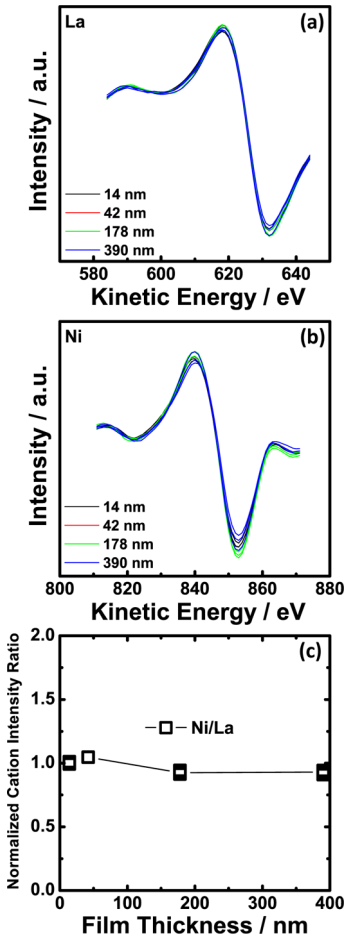

Figure 3. Ex situ AES data of the $(100)_{tetragonal}$-oriented epitaxial LNO thin films with ∼14, ∼ 42, ∼178, and ∼390 nm annealed at 550 °C in an oxygen partial pressure of 1 atm. (a) La cation variation and (b) Ni cation variation at three different locations on the LNO film surface. (c) The change of the surface Ni/La ratio as a function of film thickness. Normalized to the value obtained at ∼14 nm LNO film.

nm[38]). The LNO films have in-plane compressive strains and tensile strains normal to the film surface at room temperature (Figure S3, Supporting Information), where the magnitude of strains decreases with increasing film thickness. The strains can be attributed to the large differences in the atomic spacing values in the $(100)_{LNO}$ orientation between LNO and GDC, where lattice mismatch in the a–b plane is 0.8% (a_{LNO} = 3.862 Å[39] and $a_{LNO} = \sqrt{2}/2a_{GDC}$, a_{GDC} = 5.418 Å[40]) and that in the c plane is 9.4% (c_{LNO} = 12.685 Å[39] and $c_{LNO} = 3\sqrt{2}/2a_{GDC}$ = 11.497 Å[40]), as shown in Figure S7 (Supporting Information). The relaxed lattice parameters, $\hat{a}$ and $\hat{c}$, of LNO films at room temperature were found to not change significantly with different film thicknesses, having values in range of 3.866–3.869 Å and 12.699–12.708 Å (Figure S2, Supporting Information), respectively.

In situ heating HRXRD was conducted to show that the LNO thin films were structurally stable upon heating to 550 °C in an oxygen partial pressure of 1 atm. Upon heating to 550 °C, no phase change was observed, and only peak shifts toward low diffraction angles associated to the thermal expansion of LNO were noted, which resulted in increasing lattice parameters and relaxed unit cell volume as a function of increasing temperature, as shown in Figure 2. The volumetric thermal expansion coefficients (TECs) of the LNO thin films (11.1 × 10^{-6}∼11.9

dx.doi.org/10.1021/jp404121p | J. Phys. Chem. C 2013, 117, 18789–18795

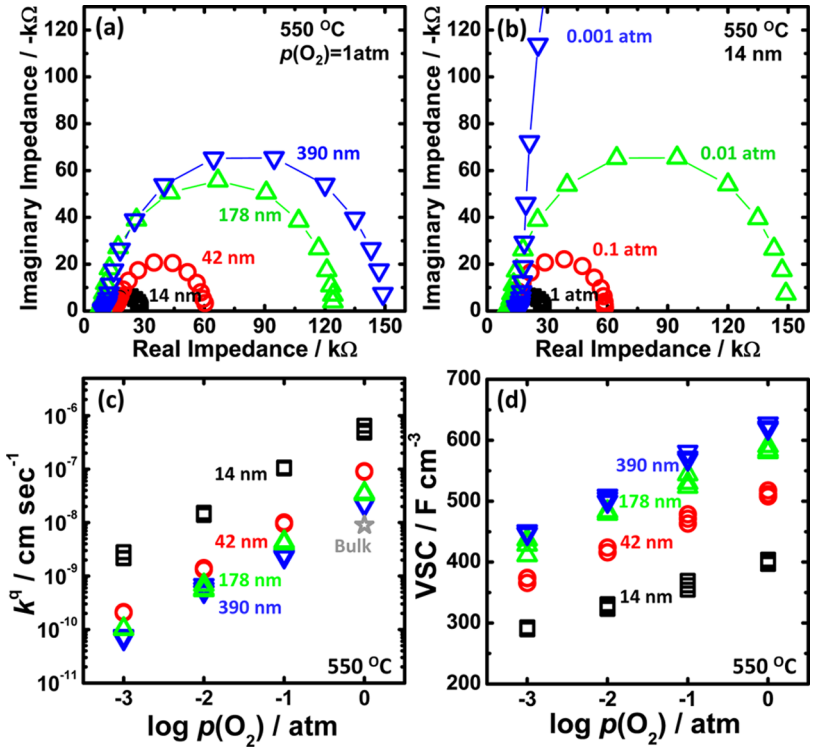

Figure 4. Electrochemical impedance spectroscopy (EIS) results of microelectrodes for the $(100)_{tetragonal}$-oriented epitaxial LNO thin films with ~14, ~ 42, ~178, and ~390 nm at 550 °C. (a) Nyquist plot of the $(100)_{tetragonal}$-oriented epitaxial LNO thin films with ~14, ~42, ~178, and ~390 nm in 1 atm $p(O_2)$. (b) Nyquist plot of the $(100)_{tetragonal}$-oriented epitaxial LNO thin films with ~14 nm as a function of $p(O_2)$. (c) Oxygen partial pressure dependency of the surface exchange coefficients, k^q, of the $(100)_{tetragonal}$-oriented epitaxial LNO thin films with ~14, ~42, ~178, and ~390 nm calculated from EIS spectra collected at 550 °C. Extrapolated bulk k^* (approximately equivalent to k^q)[41] value at 550 °C obtained from previous data of (☆-gray) Skinner et al.[30] is plotted for comparison. (d) Oxygen partial pressure dependency of volume-specific capacitance (VSC) of the $(100)_{tetragonal}$-oriented epitaxial LNO thin films with ~14, ~42, ~178, and ~390 nm calculated from EIS spectra collected at 550 °C.

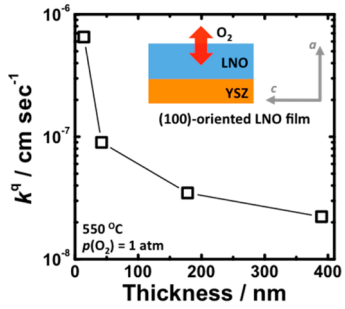

Figure 5. Thickness dependency of the k^q of the $(100)_{tetragonal}$-oriented epitaxial LNO thin films with ~14, ~42, ~178, and ~390 nm calculated from EIS spectra collected at 550 °C in 1 atm $p(O_2)$. The inset shows the schematic of the surface exchange in the $(100)_{tetragonal}$-oriented epitaxial LNO thin films.

$\times 10^{-6}$ K^{-1}) were in good agreement with those reported in the literature (11.0×10^{-6}~11.6×10^{-6} K^{-1} for bulk LNO[37]). Interestingly, the smaller relaxed unit cell volume of the LNO thin films at smaller thicknesses became increasingly evident with increasing temperature. This observation suggests that the oxygen overstoichiometry of these films decreases with decreasing film thickness at elevated temperatures, which will be discussed later.

To investigate the change of surface chemistry as a function of film thickness, ex situ AES was conducted with the LNO thin films after annealing at 550 °C in an oxygen partial pressure of 1 atm. Figures 3(a) and 3(b) show the changes in the surface La and Ni cation spectra of each film. This clearly indicates that there is no significant change in the surface La and Ni cations as a function of film thickness. The relative surface Ni/La ratios were found to be independent of film thickness (Figure 3(c)).

EIS data collected from the LNO thin films with ~14, ~42, ~178, and ~390 nm at 550 °C in an oxygen partial pressure of 1 atm are shown in Figure 4(a). The real impedance of the predominant semicircle decreased significantly with decreasing thickness of the LNO films. In addition, the predominant semicircle was found to increase with decreasing oxygen partial pressure, $p(O_2)$. Representative EIS data collected from the 14 nm film measured at 550 °C as a function of $p(O_2)$ are shown in Figure 4(b). Considering the fact that the film thicknesses are much smaller than the critical thickness (350 μm estimated for the LNO single crystal[21] at 550 °C), the $p(O_2)$-dependent impedance responses suggest that the surface oxygen exchange kinetics governs the oxygen electrocatalysis on the LNO film surface. Figure 4(c) shows the k^q of the LNO thin films with different thicknesses (~14, ~42, ~178, and ~390 nm) at 550 °C as a function of $p(O_2)$, which was obtained from the real impedance of the semicircle. The k^q values of the LNO thin films were found to decrease with increasing thickness. Assuming that k^q can be approximated as k^*,[41] it is noted that the k^q of the thinnest LNO film having a thickness of 14 nm is higher than that extrapolated for LNO bulk[30] by about 2 orders of magnitude at 1 atm. Interestingly, the trend is in contrast to no thickness dependency of k^* for the $(001)_{tetragonal}$-oriented epitaxial LNO thin films by Burriel et al.,[23] regardless of the surfaces perpendicular to either the $a-b$ plane or c-axis. The difference might be attributed to the fact that the LNO

dx.doi.org/10.1021/jp404121p | J. Phys. Chem. C 2013, 117, 18789−18795

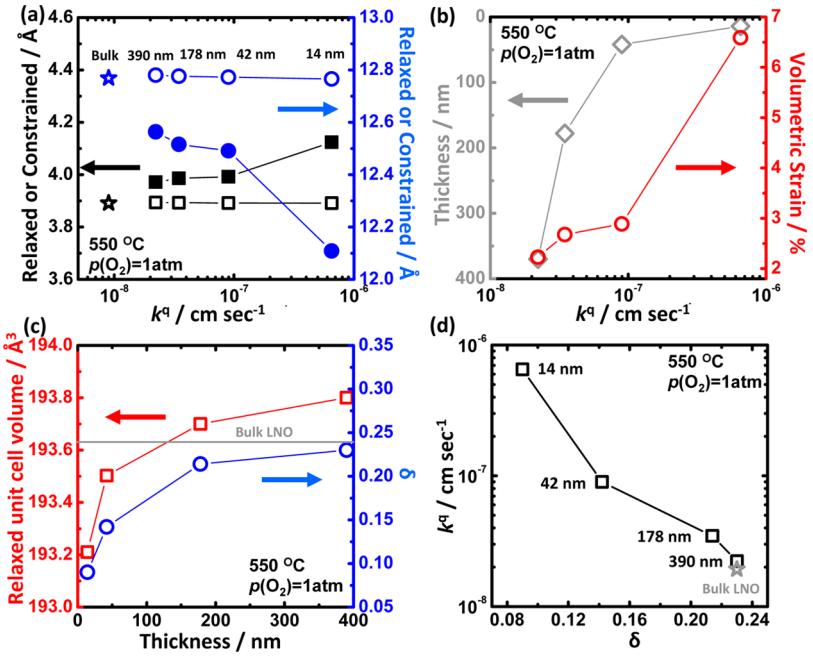

Figure 6. (a) Constrained (■-black, ●-blue) and relaxed (□-black, ○-blue) lattice parameters of the $(100)_{tetragonal}$-oriented epitaxial LNO thin films as a function of the surface oxygen exchange kinetics at 550 °C in 1 atm $p(O_2)$. Extrapolated bulk a (☆-black) and c (☆-blue) lattice parameters and the k^* value at 550 °C obtained from previous data of Skinner et al.[30,39] are plotted for comparison. (b) Thickness and volumetric strain of the $(100)_{tetragonal}$-oriented epitaxial LNO thin films as a function of the surface oxygen exchange kinetics at 550 °C in 1 atm $p(O_2)$. (c) Unit cell volume and δ extrapolated from Nakamura et al.[37] as a function of the $(100)_{tetragonal}$-oriented epitaxial LNO thin-film thickness at 550 °C in 1 atm $p(O_2)$. Extrapolated bulk unit cell volume and δ at 550 °C obtained from previous data of (gray line) Nakamura et al.[37] are plotted for comparison. (d) k^q of the $(100)_{tetragonal}$-oriented epitaxial LNO thin films as a function of δ extrapolated from Nakamura et al.[37] at 550 °C in 1 atm $p(O_2)$. Extrapolated bulk k^* value and δ obtained from previous data of (☆-gray) Skinner et al.[30] and Nakamura et al.,[37] respectively, are plotted for comparison.

thin films of previous work[23] have lower lattice mismatch with the substrate (1% on STO and −0.19% on NGO at room temperature and no high-temperature data available). On the other hand, the lattice mismatch between the $b-c$ plane parameter in the LNO thin films and GDC in this work is considerably large ($\Delta a \approx \Delta b = 6.96\%$ and $\Delta c = 4.82\%$ on GDC at room temperature and $\Delta a \approx \Delta b = 7.68\%$ and $\Delta c = 5.32\%$ at 550 °C for 14 nm film). Therefore, it is proposed that large tensile strains on the $(100)_{tetragonal}$-oriented epitaxial LNO thin films can cause the thickness-dependent k^q, as shown in Figure 5.

The greater difference between the relaxed and constrained lattice parameters of thinner LNO films was found to be accompanied by greater surface oxygen exchange kinetics, as shown in Figure 6(a). The constrained a parameters of the LNO thin films decrease very slightly with increasing film thickness, whereas the constrained c parameters increase considerably with increasing film thickness, which leads to increasing tensile volumetric strains with decreasing film thickness (Figure 6(b)). Such strains can induce changes in the oxygen nonstoichiometry, δ, in LNO. To the first approximation, the nonstoichiometry, δ, of these LNO thin films can be estimated from the unit cell volume based on the established correlation between the unit cell volume of bulk LNO and δ.[37] As the unit cell volume of the LNO thin films increases with increasing film thickness (Figure 2(b)), the extrapolated δ value of the LNO films is larger at greater thicknesses, as shown in Figure 6. The trend is further supported by the fact that volume-specific capacitances (VSCs) of LNO films extracted from EIS data (for details see the Supporting Information), which correspond to changes in δ induced by changes in the electrical potential, were found to increase with increasing film thickness, as shown in Figure 4(d). Considering that Nakamura et al.[42] have reported that the thermodynamic driving force for the formation of interstitial oxygen in bulk LNO decreases with increasing δ, it is proposed that the increasing surface oxygen exchange kinetics of thinner LNO films can be attributed to the decreasing barrier of interstitial oxygen formation and release associated with the larger thermodynamic driving force for interstitial oxygen formation at lower δ, as shown in Figure 6(d). Although the surface oxygen exchange kinetics are not correlated strongly with the electrical conductivity in LNO thin films,[23,38] the influence of hole concentration and mobility of Ni cations on the surface oxygen exchange kinetics cannot be excluded, which requires further investigation.

■ CONCLUSIONS

We have successfully deposited the $(100)_{tetragonal}$-oriented epitaxial LNO thin films with four different thicknesses. The k^q values of the LNO thin films decrease with increasing film thickness, and such a trend is not observed in $(001)_{tetragonal}$-oriented epitaxial LNO thin films.[23] Ex situ AES shows that there is no significant change of the surface chemistry as a function of film thickness before and after exposure to elevated temperatures. In situ HRXRD reveals that the unit cell volume of the LNO thin films increases with increasing film thickness at 550 °C, which indicates that oxygen nonstiochiometry, δ, in $La_2NiO_{4+\delta}$ decreases with decreasing LNO film thickness. Our results demonstrate the key role of oxygen excess of RP phases on the oxygen surface exchange process, where modifying the driving force to form interstitial oxygen by strains is a new strategy to design highly active surface oxygen exchange

dx.doi.org/10.1021/jp404121p | J. Phys. Chem. C 2013, 117, 18789−18795

materials for applications such as SOFC cathodes or oxygen-conducting membranes.

■ ASSOCIATED CONTENT

Supporting Information

Details about sample preparation, EIS testing, XRD, AFM, AES, and SEM. This material is available free of charge via the Internet at http://pubs.acs.org.

■ AUTHOR INFORMATION

Corresponding Author

*E-mail: shaohorn@mit.edu.

Notes

The authors declare no competing financial interest.

Biographies

Dongkyu Lee obtained his B.S. in Materials Science and Engineering from Hanyang University, Korea, in 2004 and his M.S. from the Gwangju Institute of Science and Technology, Korea, in 2006. Then, he worked at the Semiconductor R&D Center in Samsung Electronics Co., Ltd., Korea, until 2009. He is currently pursuing his Ph.D. at the Massachusetts Institute of Technology, USA, advised by prof. Yang Shao-Horn. His research interests include the development of the perovskite -related oxide thin films for oxygen electrocatalysis in electrochemical energy conversion devices.

Alexis Grimaud received his Physical-Chemistry Engineering diploma from the Graduate School of Chemistry and Physics of Bordeaux in 2008 and his Ph.D. from the University of Bordeaux, France, in 2011. He is currently a Postdoctoral Associate in the Electrochemical Energy Laboratory at the Massachusetts Institute of Technology, USA. His research interests focus on the development of transition metal oxides as catalysts for high and low temperature energy conversion devices.

Ethan J. Crumlin received his B.S. (2005), M.S. (2007), and Ph.D. (2012) in the department of Mechanical Engineering from the Massachusetts Institute of Technology, USA. He is currently a Postdoctoral Fellow at the Advanced Light Source at Lawrence Berkeley National Laboratory, USA. His research interests include batteries, fuel cells, and catalysis, in particular the development and utilization of in situ characterization techniques.

Khaled Mezghani received his B.S., M.S., and Ph.D. from the Department of Materials Science and Engineering at the University of Tennessee, Knoxville, USA. He is currently an Associate Professor in the Mechanical Engineering Department at KFUPM, Saudi Arabia. His research area is related to structure development and properties of materials.

Mohamed A. Habib received his Ph.D. degree in Mechanical Engineering from the Imperial College of Science and Technology, London, in 1980. He is a Professor in the Mechanical Engineering Department at KFUPM, Saudi Arabia. He has been a member in several externally funded projects and was a consultant for a number of industrial projects related to boilers and energy conservation. He has published technical papers on energy analysis, heat transfer, alternative energy, analysis of energy systems, oxyfuel combustion, carbon capture, and oxygen transport reactors. He received the distinguished researcher award in 1995 and 2010.

Zhenxing Feng received his B.S. from Peking University, China, in 2004, M.S. from McGill University, Canada, in 2006, and Ph.D. from Northwestern University, USA, in 2011. He is currently a Postdoctoral Associate in the Electrochemical Energy Laboratory at the Massachusetts Institute of Technology, USA. His research interests include the synthesis and characterization of oxide materials for applications in energy storage and conversion devices such as fuel cells and lithium batteries.

Wesley T. Hong received his B.S. in Materials Science and Engineering from Stanford University, USA, in 2011. He is currently a Ph.D. candidate in the Department of Materials Science and Engineering at the Massachusetts Institute of Technology, USA. His research interests include the solid state physics and chemistry of perovskite oxides for electrochemical energy conversion applications.

Michael D. Biegalski received his B.S. Degree from University of Illinois at Urbana−Champaign in 1998 and his M.S. and Ph.D. from Pennsylvania State University in 2002 and 2006. He currently works as a research staff scientist for the Center for Nanophase Materials Sciences at Oak Ridge National Laboratory. His current research interests focus on the control of macroscopic properties of oxide thin films through control of atomic structure.

Hans M. Christen received his M.S. and Ph.D. from the Swiss Federal Institute of Technology in Lausanne in 1991 and 1994. He is a Distinguished Research Staff Member in the Materials Science and Technology Division (MSTD) of Oak Ridge National Laboratory, with research focusing on the effects of strain, interfaces, and spatial confinement on the properties of complex oxide materials.

Yang Shao-Horn is a Gail E. Kendall Professor of Mechanical Engineering and Professor of Materials Science and Engineering at MIT. Her research is centered on understanding the electronic structures of surfaces, searching for descriptors of catalytic activity, and applying fundamental understanding to design catalysts for oxygen electrocatalysis, water splitting, and CO_2 reduction. She obtained her Ph.D. in Metallurgical and Materials Engineering from Michigan Technological University. Her select honors include Research Award of International Battery Association, Tajima Prize of the International Society of Electrochemistry, and Charles W. Tobias Young Investigator Award of the Electrochemical Society.

■ ACKNOWLEDGMENTS

This work was supported in part by DOE (SISGR DESC0002633) and King Abdullah University of Science and Technology. The authors like to thank the King Fahd University of Petroleum and Minerals in Dharam, Saudi Arabia, for funding the research reported in this paper through the Center for Clean Water and Clean Energy at MIT and KFUPM. The PLD was conducted at the Center for Nanophase Materials Sciences, which is sponsored at Oak Ridge National Laboratory by the Scientific User Facilities Division, Office of Basic Energy Sciences, U.S. Department of Energy.

■ REFERENCES

(1) da Conceicao, L.; Silva, C. R. B.; Ribeiro, N. F. P.; Souza, M. Influence of the Synthesis Method on the Porosity, Microstructure and Electrical Properties of $La_{0.7}Sr_{0.3}MnO_3$ Cathode Materials. *Mater. Charact.* **2009**, *60*, 1417−1423.

(2) De Souza, R. A.; Kilner, J. A. Oxygen Transport in $La_{1-x}Sr_xMn_{1-y}Co_yO_{3\pm\delta}$ Perovskites - Part I. Oxygen Tracer Diffusion. *Solid State Ionics* **1998**, *106*, 175−187.

(3) De Souza, R. A.; Kilner, J. A. Oxygen Transport in $La_{1-x}Sr_xMn_{1-y}Co_yO_{3\pm\delta}$ Perovskites Part Ii. Oxygen Surface Exchange. *Solid State Ionics* **1999**, *126*, 153−161.

(4) Endo, A.; Fukunaga, H.; Wen, C.; Yamada, K. Cathodic Reaction Mechanism of Dense $La_{0.6}Sr_{0.4}CoO_3$ and $La_{0.81}Sr_{0.09}MnO_3$ Electrodes for Solid Oxide Fuel Cells. *Solid State Ionics* **2000**, *135*, 353−358.

(5) Ioroi, T.; Hara, T.; Uchimoto, Y.; Ogumi, Z.; Takehara, Z. Preparation of Perovskite-Type $La_{1-x}Sr_xMnO_3$ Films by Vapor-Phase

Processes and Their Electrochemical Properties. *J. Electrochem. Soc.* **1997**, *144*, 1362−1370.
(6) Adler, S. B. Factors Governing Oxygen Reduction in Solid Oxide Fuel Cell Cathodes. *Chem. Rev.* **2004**, *104*, 4791−4843.
(7) Adler, S. B.; Chen, X. Y.; Wilson, J. R. Mechanisms and Rate Laws for Oxygen Exchange on Mixed-Conducting Oxide Surfaces. *J. Catal.* **2007**, *245*, 91−109.
(8) Jacobson, A. J. Materials for Solid Oxide Fuel Cells. *Chem. Mater.* **2010**, *22*, 660−674.
(9) Lee, Y. L.; Kleis, J.; Rossmeisl, J.; Morgan, D. Ab Initio Energetics of $LaBO_3$ (001) (B=Mn, Fe, Co, and Ni) for Solid Oxide Fuel Cell Cathodes. *Phys. Rev. B* **2009**, *80*, 224101-1−224101-20.
(10) Shao, Z. P.; Haile, S. M. A High-Performance Cathode for the Next Generation of Solid-Oxide Fuel Cells. *Nature* **2004**, *431*, 170−173.
(11) Steele, B. C. H.; Heinzel, A. Materials for Fuel-Cell Technologies. *Nature* **2001**, *414*, 345−352.
(12) Sun, C. W.; Hui, R.; Roller, J. Cathode Materials for Solid Oxide Fuel Cells: A Review. *J. Solid State Electrochem.* **2010**, *14*, 1125−1144.
(13) Hashim, S. M.; Mohamed, A. R.; Bhatia, S. Current Status of Ceramic-Based Membranes for Oxygen Separation from Air. *Adv. Colloid Interface Sci.* **2010**, *160*, 88−100.
(14) Adler, S. B. Mechanism and Kinetics of Oxygen Reduction on Porous $La_{1-x}Sr_xCoO_{3-\delta}$ Electrodes. *Solid State Ionics* **1998**, *111*, 125−134.
(15) Crumlin, E. J.; Ahn, S. J.; Lee, D.; Mutoro, E.; Biegalski, M. D.; Christen, H. M.; Shao-Horn, Y. Oxygen Electrocatalysis on Epitaxial $La_{0.6}Sr_{0.4}CoO_{3-\delta}$ Perovskite Thin Films for Solid Oxide Fuel Cells. *J. Electrochem. Soc.* **2012**, *159*, F219−F225.
(16) Crumlin, E. J.; Mutoro, E.; Liu, Z.; Grass, M. E.; Biegalski, M. D.; Lee, Y. L.; Morgan, D.; Christen, H. M.; Bluhm, H.; Shao-Horn, Y. Surface Strontium Enrichment on Highly Active Perovskites for Oxygen Electrocatalysis in Solid Oxide Fuel Cells. *Energy Environ. Sci.* **2012**, *5*, 6081−6088.
(17) la O, G. J.; Ahn, S. J.; Crumlin, E.; Orikasa, Y.; Biegalski, M. D.; Christen, H. M.; Shao-Horn, Y. Catalytic Activity Enhancement for Oxygen Reduction on Epitaxial Perovskite Thin Films for Solid-Oxide Fuel Cells. *Angew. Chem., Int. Ed.* **2010**, *49*, 5344−5347.
(18) Mizusaki, J.; Mima, Y.; Yamauchi, S.; Fueki, K.; Tagawa, H. Nonstoichiometry of the Perovskite-Type Oxides $La_{1-x}Sr_xCoO_{3-\delta}$. *J. Solid State Chem.* **1989**, *80*, 102−111.
(19) Sathe, V. G.; Pimpale, A. V.; Siruguri, V.; Paranjpe, S. K. Neutron Diffraction Studies of Perovskite-Type Compounds $La_{1-x}Sr_xCoO_3$ (x=0.1, 0.2, 0.3, 0.4, 0.5). *J. Phys.: Condens. Matter* **1996**, *8*, 3889−3896.
(20) Wang, S. Y.; Yoon, J.; Kim, G.; Huang, D. X.; Wang, H. Y.; Jacobson, A. J. Electrochemical Properties of Nanocrystalline $La_{0.5}Sr_{0.5}CoO_{3-\delta}$ Thin Films. *Chem. Mater.* **2010**, *22*, 776−782.
(21) Bassat, J. M.; Odier, P.; Villesuzanne, A.; Marin, C.; Pouchard, M. Anisotropic Ionic Transport Properties in $La_2NiO_{4+\delta}$ Single Crystals. *Solid State Ionics* **2004**, *167*, 341−347.
(22) Boehm, E.; Bassat, J. M.; Dordor, P.; Mauvy, F.; Grenier, J. C.; Stevens, P. Oxygen Diffusion and Transport Properties in Non-Stoichiometric $Ln_{(2-x)}NiO_{(4+\delta)}$ Oxides. *Solid State Ionics* **2005**, *176*, 2717−2725.
(23) Burriel, M.; Garcia, G.; Santiso, J.; Kilner, J. A.; Richard, J. C. C.; Skinner, S. J. Anisotropic Oxygen Diffusion Properties in Epitaxial Thin Films of La2nio4+Delta. *J. Mater. Chem.* **2008**, *18*, 416−422.
(24) Chroneos, A.; Parfitt, D.; Kilner, J. A.; Grimes, R. W. Anisotropic Oxygen Diffusion in Tetragonal $La_2NiO_{4+\delta}$: Molecular Dynamics Calculations. *J. Mater. Chem.* **2010**, *20*, 266−270.
(25) Cleave, A. R.; Kilner, J. A.; Skinner, S. J.; Murphy, S. T.; Grimes, R. W. Atomistic Computer Simulation of Oxygen Ion Conduction Mechanisms in $La_2NiO_{4+\delta}$. *Solid State Ionics* **2008**, *179*, 823−826.
(26) Garcia, G.; Burriel, M.; Bonanos, N.; Santiso, J. Electrical Conductivity and Oxygen Exchange Kinetics of $La_2NiO_{4+\delta}$ Thin Films Grown by Chemical Vapor Deposition. *J. Electrochem. Soc.* **2008**, *155*, P28−P32.
(27) Kharton, V. V.; Viskup, A. P.; Naumovich, E. N.; Marques, F. M. B. Oxygen Ion Transport in La_2NiO_4-Based Ceramics. *J. Mater. Chem.* **1999**, *9*, 2623−2629.
(28) Kilner, J. A.; Shaw, C. K. M. Mass Transport in $La_2Ni_{1-x}Co_xO_{4+\delta}$ Oxides with the K_2NiF_4 Structure. *Solid State Ionics* **2002**, *154*, 523−527.
(29) Kim, G.; Wang, S.; Jacobson, A. J.; Chen, C. L. Measurement of Oxygen Transport Kinetics in Epitaxial $La_2NiO_{4+\delta}$ Thin Films by Electrical Conductivity Relaxation. *Solid State Ionics* **2006**, *177*, 1461−1467.
(30) Skinner, S. J.; Kilner, J. A. Oxygen Diffusion and Surface Exchange in $La_{2-x}Sr_xNiO_{4+\delta}$. *Solid State Ionics* **2000**, *135*, 709−712.
(31) Crumlin, E. J.; Mutoro, E.; Ahn, S. J.; Jose la O′, G.; Leonard, D. N.; Borisevich, A.; Biegalski, M. D.; Christen, H. M.; Shao-Horn, Y. Oxygen Reduction Kinetics Enhancement on a Heterostructured Oxide Surface for Solid Oxide Fuel Cells. *J. Phys. Chem. Lett.* **2010**, *1*, 3149−3155.
(32) Mutoro, E.; Crumlin, E. J.; Biegalski, M. D.; Christen, H. M.; Shao-Horn, Y. Enhanced Oxygen Reduction Activity on Surface-Decorated Perovskite Thin Films for Solid Oxide Fuel Cells. *Energy Environ. Sci.* **2011**, *4*, 3689−3696.
(33) Yamada, A.; Suzuki, Y.; Saka, K.; Uehara, M.; Mori, D.; Kanno, R.; Kiguchi, T.; Mauvy, F.; Grenier, J. C. Ruddlesden-Popper-Type Epitaxial Film as Oxygen Electrode for Solid-Oxide Fuel Cells. *Adv. Mater.* **2008**, *20*, 4124−4128.
(34) Jorgensen, J. D.; Dabrowski, B.; Pei, S.; Richards, D. R.; Hinks, D. G. Structure of the Interstitial Oxygen Defect in $La_2NiO_{4+\delta}$. *Phys. Rev. B* **1989**, *40*, 2187−2199.
(35) Demourgues, A.; Weill, F.; Darriet, B.; Wattiaux, A.; Grenier, J. C.; Gravereau, P.; Pouchard, M. Additional Oxygen Ordering in $La_2NiO_{4.25}$ ($La_8Ni_4O_{17}$). 1. Electron and Neutron-Diffraction Study. *J. Solid State Chem.* **1993**, *106*, 317−329.
(36) Rodriguezcarvajal, J.; Fernandezdiaz, M. T.; Martinez, J. L. Neutron-Diffraction Study on Structural and Magnetic-Properties of La_2NiO_4. *J. Phys.: Condens. Matter* **1991**, *3*, 3215−3234.
(37) Nakamura, T.; Yashiro, K.; Sato, K.; Mizusaki, J. Structural Analysis of $La_{2-x}Sr_xNiO_{4+\delta}$ by High Temperature X-Ray Diffraction. *Solid State Ionics* **2010**, *181*, 292−299.
(38) Burriel, M.; Santiso, J.; Rossell, M. D.; Van Tendeloo, G.; Figueras, A.; Garcia, G. Enhancing Total Conductivity of $La_2NiO_{4+\delta}$ Epitaxial Thin Films by Reducing Thickness. *J. Phys. Chem. C* **2008**, *112*, 10982−10987.
(39) Skinner, S. J. Characterisation of $La_2NiO_{4+\delta}$ Using in-Situ High Temperature Neutron Powder Diffraction. *Solid State Sci.* **2003**, *5*, 419−426.
(40) Matovic, B.; Boskovic, S.; Zivkovic, L.; Vlajic, M.; Krstic, V. Lattice Parameters of Gd-Doped Ceria Electrolytes. In *Current Research in Advanced Materials and Processes*; Uskokovic, D. P., Milonjic, S. K., Rakovic, D. I., Eds.; Trans Tech Publications Ltd.: Zurich-Uetikon, 2005; Vol. *494*, pp 175−179.
(41) Maier, J. On the Correlation of Macroscopic and Microscopic Rate Constants in Solid State Chemistry. *Solid State Ionics* **1998**, *112*, 197−228.
(42) Nakamura, T.; Yashiro, K.; Sato, K.; Mizusaki, J. Oxygen Nonstoichiometry and Defect Equilibrium in $La_{2-x}Sr_xNiO_{4+\delta}$. *Solid State Ionics* **2009**, *180*, 368−376.